

Article

# Chemically and Physically Cross-Linked Inorganic–Polymer Hybrid Solvent-Free Electrolytes

Yamato Kanai <sup>1</sup>, Koji Hiraoka <sup>1</sup>, Mutsuhiro Matsuyama <sup>2</sup> and Shiro Seki <sup>1,\*</sup> 

<sup>1</sup> Graduate School of Applied Chemistry and Chemical Engineering, Kogakuin University, 2665-1 Nakano-machi, Hachioji-city, Tokyo 192-0015, Japan; bm21013@g.kogakuin.jp (Y.K.); bd21002@ns.kogakuin.ac.jp (K.H.)

<sup>2</sup> Sumitomo Bakelite Co., Ltd., 5-8 Higashi-Shinagawa 2-Chome, Shinagawa-ku, Tokyo 140-0002, Japan; matuyama@sumibe.co.jp

\* Correspondence: shiro-seki@cc.kogakuin.ac.jp; Tel.: +81-42-628-4568

**Abstract:** Safe, self-standing, all-solid-state batteries with improved solid electrolytes that have adequate mechanical strength, ionic conductivity, and electrochemical stability are strongly desired. Hybrid electrolytes comprising flexible polymers and highly conductive inorganic electrolytes must be compatible with soft thin films with high ionic conductivity. Herein, we propose a new type of solid electrolyte hybrid comprising a glass–ceramic inorganic electrolyte powder ( $\text{Li}_{1+x+y}\text{Al}_x\text{Ti}_{2-x}\text{Si}_y\text{P}_{3-y}\text{O}_{12}$ ; LICGC) in a poly(ethylene)oxide (PEO)-based polymer electrolyte that prevents decreases in ionic conductivity caused by grain boundary resistance. We investigated the cross-linking processes taking place in hybrid electrolytes. We also prepared chemically cross-linked PEO/LICGC and physically cross-linked poly(norbornene)/LICGC electrolytes, and evaluated them using thermal and electrochemical analyses, respectively. All of the obtained electrolyte systems were provided with homogenous, white, flexible, and self-standing thin films. The main ionic conductive phase changed from the polymer to the inorganic electrolyte at low temperatures (close to the glass transition temperature) as the LICGC concentration increased, and the  $\text{Li}^+$  ion transport number also improved. Cyclic voltammetry using [Li metal | Ni] cells revealed that Li was reversibly deposited/dissolved in the prepared hybrid electrolytes, which are expected to be used as new  $\text{Li}^+$ -conductive solid electrolyte systems.

**Keywords:** polymer electrolyte; all-solid-state battery; ionic conductivity; interfacial resistance; grain boundary; activation energy



**Citation:** Kanai, Y.; Hiraoka, K.; Matsuyama, M.; Seki, S. Chemically and Physically Cross-Linked Inorganic–Polymer Hybrid Solvent-Free Electrolytes. *Batteries* **2023**, *9*, 492. <https://doi.org/10.3390/batteries9100492>

Received: 7 August 2023

Revised: 8 September 2023

Accepted: 20 September 2023

Published: 26 September 2023



**Copyright:** © 2023 by the authors. Licensee MDPI, Basel, Switzerland. This article is an open access article distributed under the terms and conditions of the Creative Commons Attribution (CC BY) license (<https://creativecommons.org/licenses/by/4.0/>).

## 1. Introduction

Energy storage technologies that save energy, have a low environmental impact, and use diverse supply sources are in demand. Li-ion batteries (LIBs) have become important parts of our daily lives, and are widely used in applications such as smartphones and electric vehicles. Moreover, it is expected that they will be used more widely in large-scale electric power storage with photovoltaic and wind power technologies [1,2]. Flammable organic solvents are mainly used as the electrolytes for LIBs, but there are concerns about liquid leakage and fire hazards [3]. Therefore, in recent years, all-solid-state Li batteries (ASSBs) using a nonflammable electrolyte layer (inorganic and organic polymer systems) have been energetically investigated instead of conventional liquid electrolytes [4–8]. A major topic of research for the synthesis and evaluation of solid electrolytes (SEs) is inorganic electrolyte systems comprising oxide- or sulfide-based SEs. Sulfide-based SEs have quite high ionic conductivities, but have relatively low chemical stability in air and are expensive to produce [9,10]. In contrast, oxide-based SEs are relatively safe owing to their high chemical stability, and perovskite-type  $\text{La}_{2/3-x}\text{Li}_{3x}\text{TiO}_3$  (LLTO) [11] and garnet-type  $\text{Li}_7\text{La}_3\text{Zr}_2\text{O}_{12}$  (LLZO) [12] have relatively high ionic conductivities (the order of  $10^{-4} \text{ S cm}^{-1}$ ) at room temperature. However, oxide-based SEs have a large resistance component caused by their

grain boundaries ( $R_{GB}$ ). Moreover, they exhibit poor adhesion properties with regard to other components (e.g., electrode layers) and consequently form inadequate interfaces. In general, the  $R_{GB}$  is the dominant resistance component of polycrystalline oxide-based SEs, and the effective ionic conductivity of an SE decreases to 1–2 digits lower than that of its bulk phase [13]. Glass ceramic (GC) SEs, prepared via crystal deposition onto a glass base material, have been proposed as possible materials for the control of the  $R_{GB}$  [14,15]. In such an arrangement, a glass phase exists between grains, and relatively high ionic conductivity is possible. A comparison between “glass” and a “crushed glass pellet” confirmed almost the same apparent activation energy, and suggested a negligible  $R_{GB}$  [16–18]. In contrast, organic polymer SEs containing polyether-based polymer chains are also reported as soft and self-standing electrolytes, and enable the formation of adhesive thin films with adequate electrode interfaces [19–21]. Some of the best-known SEs, i.e., poly(ethylene)oxide (PEO)-based SEs, have relatively low ionic conductivities of the order of  $10^{-4}$  S  $\text{cm}^{-1}$  at 333 K. Therefore, improvements to the ionic conductivity of such electrodes are needed if they are to be used in ASSBs [22]. In an attempt to improve the ionic conductivity of polymer-based SEs, branched side chains have been introduced into the main chain because there are differences in the relaxation times between the main chain ( $\alpha$  relaxation) and the side chains ( $\beta$  relaxation), which relax more quickly [23]. Recently, hybrid SEs containing both inorganic and polymer phases have been reported. The aim of this design is to achieve the high flexibility and ionic conductivity that are required for ASSBs [24–27]. Although PEO/LLZO hybrid systems with relatively high ionic conductivities ( $10^{-5}$  to  $10^{-4}$  S  $\text{cm}^{-1}$  at room temperature) have been reported [28,29], significant improvements in ionic conductivities have not been confirmed in the case of SE compositions with high (e.g., more than 50 wt.%) levels of inorganic materials [30,31]. A rise in the  $R_{GB}$  due to the continuous inorganic (powder) phase and the interfacial resistance between the polymer/inorganic SEs have been suggested as possible causes of the increase in resistance.

In the present study, we produced hybrid SEs comprising a suitable soft and rubbery polymer and an oxide-based inorganic powder to achieve high  $\text{Li}^+$  conductivity. Chemically cross-linked branched PEO-based SEs and physically cross-linked poly(norbornene-co-ether) SEs [32] were used as the polymer phase, and  $\text{Li}_{1+x+y}\text{Al}_x\text{Ti}_{2-x}\text{Si}_y\text{P}_{3-y}\text{O}_{12}$  (LICGC) Na super ionic conductor (NASICON)-type GC SEs were used as the inorganic phase to prepare hybrid SEs. The thermal, ionic conductivity, and electrochemical (interfacial stability with Li metal and  $\text{Li}^+$  transport number) properties of the prepared hybrid SEs were evaluated, and the effects of the polymer structures on the hybrid SEs were investigated.

## 2. Experimental Procedure

### 2.1. Preparation of P(EO/PO)/LICGC and P(EO/PO)-PEO<sub>3</sub>/LICGC Composite Electrolytes

All sample preparations were conducted in a dry argon-filled glove box ( $[\text{O}_2] < 10$  ppm, dew point  $< 193$  K, Miwa Mfg Co., Ltd., Osaka, Japan). P(EO/PO) (EO = ethylene oxide; PO = propylene oxide; ratio of EO:PO = ca. 8:2;  $M_w$ : ca. 8000; Dai-ich Kogyo Seiyaku Co., Kyoto, Japan) and P(EO/PO)-PEO<sub>3</sub> (PEO<sub>3</sub>;  $M_w$ : ca. 350; Dai-ich Kogyo Seiyaku Co.) were used as a matrix polymer, and  $\text{LiN}(\text{SO}_2\text{CF}_3)_2$  (LiTFSA, Solvay Japan Co., Ltd., Tokyo, Japan) was also added as a dissolved salt. The P(EO/PO)/ $\text{Li}_2\text{O}-\text{Al}_2\text{O}_3-\text{SiO}_2-\text{P}_2\text{O}_5-\text{TiO}_2$ -based inorganic electrolyte ( $\text{Li}_{1+x+y}\text{Al}_x\text{Ti}_{2-x}\text{Si}_y\text{P}_{3-y}\text{O}_{12}$ , LICGC, Ohara Co., Kanagawa, Japan) and branched P(EO/PO)-PEO<sub>3</sub>/LICGC were prepared via the photo-initiated polymerization of a P(EO/PO) acrylate macromonomer using 2,2 dimethoxy-2-phenylacetophenone (DMPA) as a photo initiator. In addition, methoxytriethylene glycol acrylate (PEO<sub>3</sub>) was added as a side chain with a free terminal (40 wt% of P(EO/PO)). LiTFSA ( $[\text{Li}]/[\text{O}] = 0.10$  per mole of oxygen units of P(EO/PO)) and DMPA (0.1 wt% of P(EO/PO)) were dissolved in a mixed solution, and LICGC powder was added to the solution. The composition percentages of LICGC ( $x$ ) were 0, 50, 100, and 150 wt% of P(EO/PO) or P(EO/PO)-PEO<sub>3</sub>. Acetonitrile was added to obtain a homogeneous solution of P(EO/PO)/LICGC. The P(EO/PO)/LICGC was dried under vacuum for 12 h to completely remove the acetonitrile. The mixtures were spread between two glass plates separated by a 0.1 mm thick Teflon

sheet. P(EO/PO)/LICGC and P(EO/PO)-PEO<sub>3</sub>/LICGC composite thin films (0.1 mm thick) were also fabricated via irradiation with ultraviolet light for 5 min to achieve the cross-linking of P(EO/PO).

## 2.2. Preparation of P(NB/G2)/LICGC Composite Electrolytes

We obtained physically cross-linkable norbornene/di-methylene-glycol di-methyl ether (P(NB/G2) as a ring monomer ( $M_w = \text{ca. } 14,000$ ; Sumitomo Bakelite Co., Ltd., Tokyo, Japan), LiTFSA ([Li]/[O] = 0.10), and LICGC. The composition percentages of LICGC ( $x$ ) were 0, 50, and 100 wt% of P(NB/G2). Acetonitrile was added to the prepared mixture to obtain a homogeneous solution. The solution was cast onto a glass plate and left stationary at ambient temperature for 8 h. The acetonitrile was then completely removed on a hot plate at 373 K for 1 h. Composite thin films comprising P(NB/G2)/LICGC were obtained by spreading the dried slurry mixture on polyethylene terephthalate films to a defined thickness of 0.1 mm using a glass plate.

## 2.3. Physical Properties of P(EO/PO)/LICGC, P(PO/EO)-PEO<sub>3</sub>/LICGC, and P(NB/G2)/LICGC

Cross-sectional images of the P(EO/PO)/LICGC and P(NB/G2)/LICGC composite electrolytes were investigated using scanning electron microscopy and energy-dispersive X-ray spectroscopy (SEM/EDX, JCM 6000, JEOL, Tokyo, Japan). The glass transition temperatures ( $T_g$ s) of each composite solid electrolyte were measured via differential scanning calorimetry (DSC; Thermo plus EVO2 DSC8231, Rigaku, Tokyo, Japan) under a N<sub>2</sub> atmosphere. Prior to obtaining the DSC measurements, each composite solid film was tightly sealed in an aluminum pan in the dry glove box. The DSC measurements were conducted by cooling the samples to 173 K, then heating them at 10 K min<sup>-1</sup>. The  $T_g$  values were determined at the middle point of the heat capacity change in the DSC thermograms during the heating step.

## 2.4. Electrochemical Properties of P(EO/PO)/LICGC, P(PO/EO)-PEO<sub>3</sub>/LICGC, and P(NB/G2)/LICGC

The ionic conductivity ( $\sigma$ ) of each composite solid electrolyte was measured via AC impedance spectroscopy (VSP, Bio Logic). The composite electrolyte films were cut into circles with diameters ( $\phi$ ) of 12 mm, each of which was sandwiched between two stainless steel plate blocking electrodes and encapsulated in a measurement cell to prevent exposure to the air. The measurements were obtained at 200 kHz to 50 mHz at 100 mV above 263.15 K and 500 mV below 258.2 K. All samples were thermally equilibrated for 1.5 h at each temperature before obtaining the AC impedance measurements.

We obtained AC impedance measurements to determine the chemical stability of [Li | electrolyte | Li] symmetrical cells and the temperature dependence of electrolyte/Li metal electrode interfacial resistance. The prepared P(PO/EO)/LICGC and P(PO/EO)-PEO<sub>3</sub>/LICGC films were sandwiched between two Li metal electrodes and encapsulated as 2032-type coin cells in the glove box. The time dependencies of resistance in the symmetrical cells were evaluated in the frequency range of 200 kHz to 10 mHz at amplitudes of 100 or 300 mV. The coin cells were stored at 333.2 K, and their impedance spectra were obtained every 5 h. The temperature dependencies of the impedance spectra were determined in the frequency range of 200 kHz to 50 mHz at an amplitude of 100 mV above 263.2 K, and at 500 mV below 258.2 K as the cells were cooled from 353.2 K. The Li<sup>+</sup> transport number ( $t_+$ ) values of P(PO/EO)/LICGC and P(PO/EO)-PEO<sub>3</sub>/LICGC were measured via AC impedance spectroscopy using [Li | electrolyte | Li] symmetrical cells. The measurements were obtained at 333.2 K in the frequency range of 200 kHz to 10  $\mu$ Hz at amplitudes of 100 or 300 mV.

We investigated the Li deposition/dissolution properties of a [Li | P(NB/G2)/LICGC | Ni] cell via cyclic voltammetry. The P(NB/G2)/LICGC films were cut into circles with diameters ( $\phi$ ) of 12 mm, each of which was sandwiched between a Ni plate working electrode and a Li foil counter/reference electrode and encapsulated in a measurement

cell to prevent exposure to the air. Cyclic voltammetry was carried out at 303.2 K at a scan rate of  $2.0 \text{ mV min}^{-1}$  over a voltage range of  $-1.0$  to  $2.5 \text{ V}$  versus  $\text{Li/Li}^+$  from an open-circuit voltage.

### 3. Results and Discussion

#### 3.1. SEM Images of the Polymer/LICGC Composite Solid Electrolyte

Figure 1 shows the P(EO/PO)/LICGC (a) and P(NB/G2) (b) ( $x = 100$ ) samples at room temperature. The samples were white, owing to the LICGC dispersed in the polymer matrix. They were highly flexible but self-standing, and had sufficient mechanical strength to form interfaces with electrode materials. Figure 1c,d shows cross-sectional SEM images of the P(EO/PO)/LICGC and P(NB/G2)/LICGC samples, and Figure 1e–h shows the cross-sectional EDX mapping of elemental S in LiTFSa and P in LICGC. Bright areas with dimensions in the order of a few micrometers were observed throughout the cross-sectional SEM images, and P was estimated to correspond to the LICGC particles in the EDX spectra. Therefore, prominent agglomerates were not apparent in the P(EO/PO)/LICGC or P(NB/G2)/LICGC samples. The LICGC particles were highly dispersible in the polymer phase at the relatively high composite ratio of  $x = 100$ , proving that they were suitable for the fabrication of homogeneous composite solid electrolyte membranes.

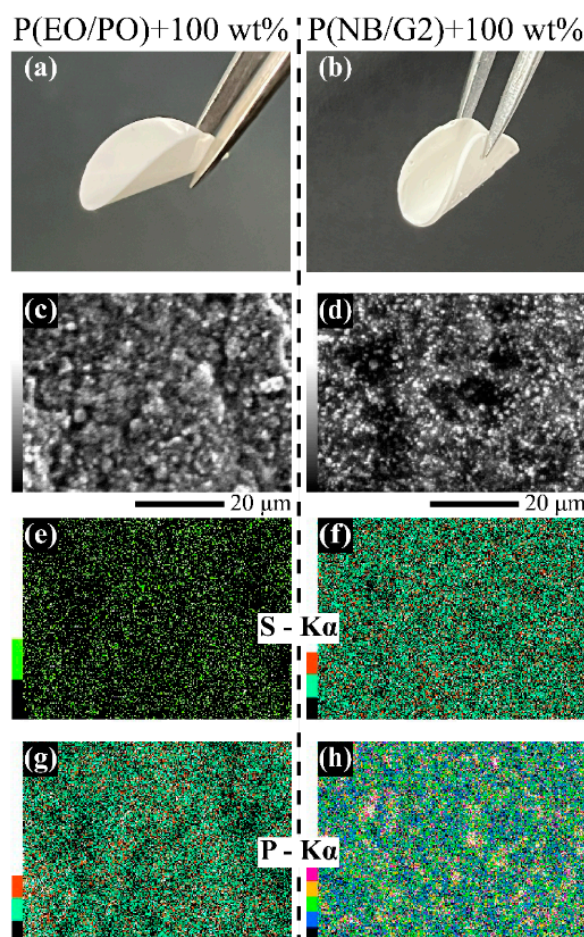


**Figure 1.** Photographs of P(EO/PO) + 100 wt% LICGC (a) and P(NB/G2) + 100 wt% LICGC (b). Cross-sectional SEM images of P(EO/PO) + 100 wt% LICGC (c) and P(NB/G2) + 100 wt% LICGC (d). EDX mapping images for S (e,f) and P (g,h) in P(EO/PO) + 100 wt% LICGC and P(NB/G2) + 100 wt% LICGC (EO = ethylene oxide; PO = propylene oxide; LICGC =  $\text{Li}_{1+x+y}\text{Al}_x\text{Ti}_{2-x}\text{Si}_y\text{P}_{3-y}\text{O}_{12}$ ; SEM = scanning electron microscopy; NB/G2 = norbornene/dimethylene-glycol di-methyl ether; EDX = energy-dispersive X-ray spectroscopy).

### 3.2. Thermal Properties of P(EO/PO)/LICGC, P(PO/EO)-PEO<sub>3</sub>/LICGC, and P(NB/G2)/LICGC

Figure 2a shows the DSC thermograms of P(EO/PO)/LICGC and P(PO/EO)-PEO<sub>3</sub>/LICGC. Each sample experienced a thermal transition at the  $T_g$  of the polymer electrolyte, i.e., at approximately 230–250 K. Figure 2b shows the DSC thermograms of the P(NB/G2)/LICGC hybrid electrolyte. Each sample experienced a slight thermal transition at approximately 260–280 K, which was attributable to the thermal vibration of the ether chain in the G2 unit. The G2 unit may require less energy for molecular motion than the NB unit. Therefore, the thermal vibrations occurred at low temperatures and may not have appeared as clear thermal transitions. Furthermore, in contrast to the PEO-based composite solid electrolytes, each P(NB/G2) electrolyte exhibited a heat capacity change, which could be attributable to the glass transition of the NB unit at 290–310 K. The  $T_g$  reflects the properties of the host polymer in the composite solid electrolyte. There was a heat capacity change at approximately 310–330 K, which may be attributed to the softening of the NB unit. Figure 2c shows the relationships between  $x$  and  $T_g$  in the fabricated P(EO/PO)/LICGC, P(EO/PO)-PEO<sub>3</sub>/LICGC, and P(NB/G2)/LICGC samples. The order of  $T_g$  for  $x = 0$  (pure polymer electrolyte) was P(EO/PO)-PEO<sub>3</sub> < P(EO/PO) < P(NB/G2)/LICGC, and the  $T_g$  of P(EO/PO)-PEO<sub>3</sub> was approximately 10 K lower than that of P(EO/PO). The decrease in the  $T_g$  may be attributed to the slight increase in the free volume of the polymer phase caused by the introduction of highly mobile low-molecular-weight free chains. In addition, the  $T_g$  value of P(NB/G2) was more than 50 K higher than the values of the PEO-based electrolytes. Physically cross-linked P(NB/G2) is considered more thermally stable than chemically cross-linked polymers consisting mainly of EO units, because the hard physical cross-linking points of the NB units and the soft ion conducting G2 units provide an intramolecular phase separation framework. The  $T_g$  values of the P(EO/PO)-PEO<sub>3</sub>/LICGC samples did not change significantly with the LICGC concentration, suggesting that the free volume and segmental motion were maintained [33,34]. The  $T_g$  of P(NB/G2)/LICGC decreased slightly with the LICGC concentration; the introduction of LICGC particles into P(NB/G2) may have increased its free volume and decreased its  $T_g$  by changing its surface properties. Therefore, the difference in the  $T_g$  values between PEO-based composites and P(NB/G2)/LICGC solid electrolytes is considered an indication of differences between the polymer structures of their hosts.

### 3.3. Ionic Conductivity Properties of P(EO/PO)/LICGC, P(PO/EO)-PEO<sub>3</sub>/LICGC, and P(NB/G2)/LICGC

Figure 3 shows the relationship between the temperature and  $\sigma$  in P(EO/PO)/LICGC (Table S1), P(EO/PO)-PEO<sub>3</sub>/LICGC (Table S2), and P(NB/G2)/LICGC (Table S3). The majority of ionic conduction occurred in the polymer phase because  $\sigma$  had a non-Arrhenius temperature dependency similar to that of pure PEO-based solid electrolytes at high temperatures. The  $\sigma$  of P(EO/PO)/LICGC decreased with the LICGC concentration over the entire temperature range. We considered that a polymer–particle interface formed within P(EO/PO)/LICGC; the resistance can be attributed to the grain boundaries between the LICGC particles ( $R_{GB}$ ), which contributed to the decrease in  $\sigma$ . In addition, the temperature dependence of  $\sigma$  in the low-temperature range tended to be linear. This behavior implies that Li<sup>+</sup> was preferentially conducted in the LICGC phase [30] in the low-temperature range.

At temperatures below approximately 283 K, the  $\sigma$  value of P(EO/PO)-PEO<sub>3</sub>/LICGC when  $x = 50$  or 100 was higher than when  $x = 0$ . In P(EO/PO)-PEO<sub>3</sub>/LICGC and P(EO/PO)/LICGC, Li<sup>+</sup> conductivity was greatest in the continuous phase of LICGC in the low-temperature range, and the transport process at the polymer/particle interface may have been promoted by the high mobility of the free chains. The  $\sigma$  of P(NB/G2)/LICGC was decreased by the introduction of LICGC. This was caused by the formation of a continuous LICGC phase following the introduction of LICGC. In P(NB/G2)/LICGC ( $x = 0$ ),  $\sigma$  was observed to decrease to 283 K, but was observed to decrease to 263 K after the introduction of LICGC, which suggests that Li<sup>+</sup> conduction occurred mainly in the LICGC phase below 278 K. Therefore,

the introduction of LICGC to solid polymer electrolytes promotes ionic conduction in the low-temperature range, and is expected to contribute to the low-temperature actuation of all-solid-state batteries.

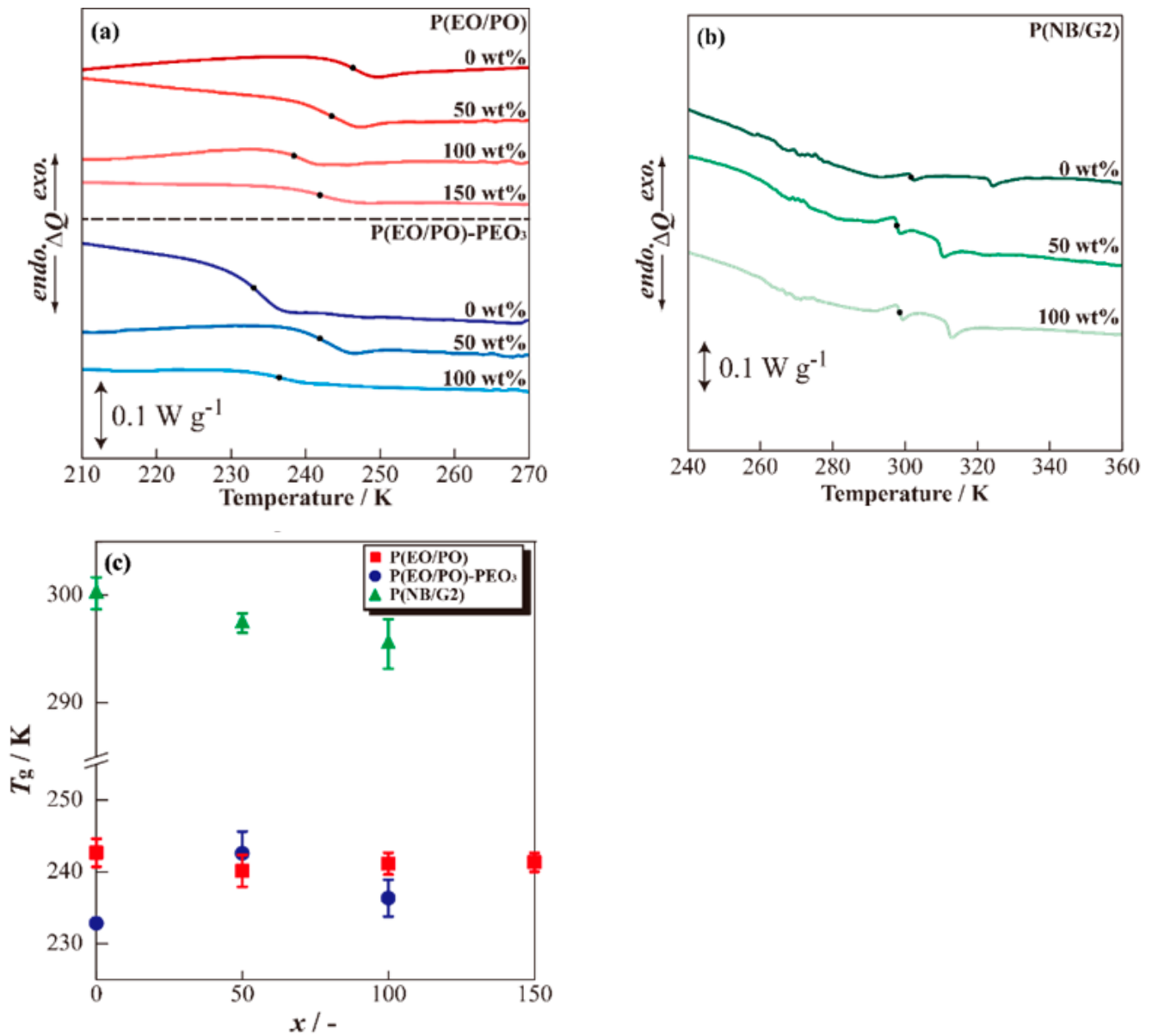


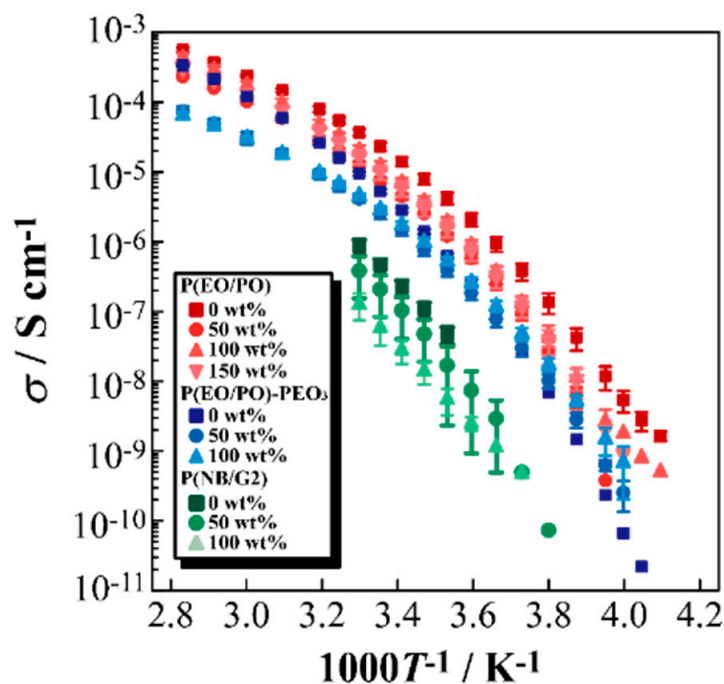
**Figure 2.** DSC thermograms of P(EO/PO)/LICGC and P(EO/PO)-PEO<sub>3</sub>/LICGC (a), P(NB/G2)/LICGC composite electrolytes (b) during the heating process, and  $x$  dependence of glass transition temperature ( $T_g$ ) (c) (EO = ethylene oxide; PO = propylene oxide; LICGC =  $\text{Li}_{1+x+y}\text{Al}_x\text{Ti}_{2-x}\text{Si}_y\text{P}_{3-y}\text{O}_{12}$ ; NB/G2 = norbornene/di-methylene-glycol di-methyl ether).

### 3.4. [Li|Composite Solid Electrolyte|Li] Symmetrical Cells

We investigated the time dependency of the electrolyte–Li metal interfacial resistance ( $R_{\text{Li}}$ ) to evaluate the electrochemical stabilities of the P(EO/PO)/LICGC and P(EO/PO)-PEO<sub>3</sub>/LICGC electrolytes, as shown in Figure 4. The Nyquist plots obtained from the [Li|composite solid electrolyte|Li] symmetrical cells were analyzed using an equivalent circuit described by Equation (1), and the  $R_{\text{Li}}$  was calculated by separating the resistive components:

$$R_b + Q_{\text{Li}}/R_{\text{Li}} + Q_{\text{diff}} \quad (1)$$

where  $R_b$  is the bulk resistance of the electrolyte, and  $Q_{Li}$  and  $R_{Li}$  are the capacitance and resistance caused by the charge transfer of  $Li^+$ , respectively. The  $R_{Li}$  values of both composite solid electrolytes remained almost constant for approximately 200 h, and a stable interface formed with the Li metal electrode. Although polyether-based polymer solid electrolytes form stable interfaces with Li metal electrodes by virtue of their high electrochemical stability, the Ti in LICGC reportedly forms an unstable interface by reacting with Li metal [35]. In the present study, the LICGC particles in the composite solid electrolytes were covered by the polymer phase, which prevented direct contact with the Li metal electrode, and would have formed a stable interface. This suggests that even a composite solid electrolyte containing Ti may be applicable to an all-solid-state battery containing a Li metal electrode. In addition, the  $R_{Li}$  of the P(EO/PO)/LICGC sample had a minimum value at  $x = 100$ , and the maximum value at  $x = 150$  corresponded to a slight side reaction in the LICGC phase. In the case of a relatively low LICGC concentration of  $x = 0$ –100, the continuous phase of LICGC formed close to the electrolyte–Li metal interface, and may have promoted  $Li^+$  transport and reduced the  $R_{Li}$ . Furthermore, when PEO<sub>3</sub> was introduced, the  $R_{Li}$  values were slightly lower when  $x = 50$  or 100 than when  $x = 0$ . This implies that the enhancement of  $Li^+$  transport at the polymer/LICGC particle interface contributes to a reduction in  $R_{Li}$ .



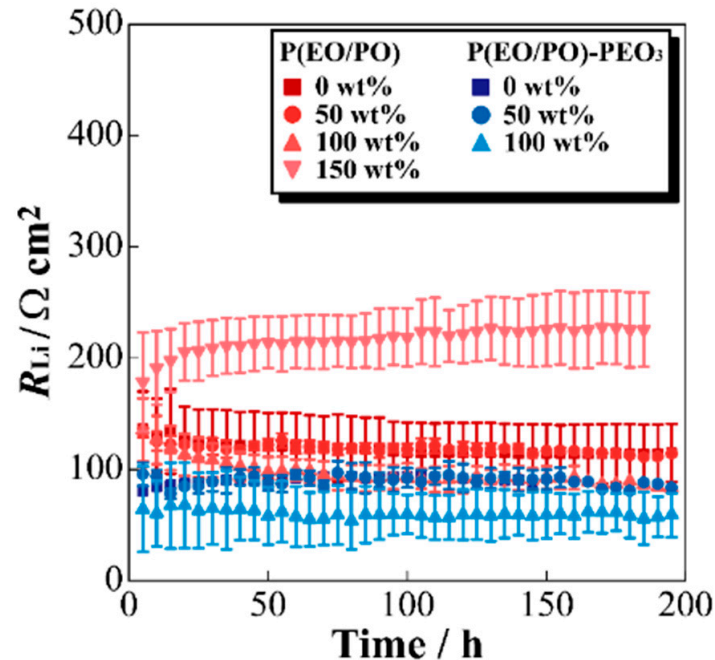
**Figure 3.** Temperature dependence of ionic conductivity ( $\sigma$ ) in the P(EO/PO)/LICGC and P(NB/G2)/LICGC composite electrolytes (EO = ethylene oxide; PO = propylene oxide; LICGC =  $Li_{1+x+y}Al_xTi_{2-x}Si_yP_{3-y}O_{12}$ ; NB/G2 = norbornene/di-methylene-glycol di-methyl ether).

Figure 5a,b shows the Cole–Cole plots of [Li | P(EO/PO)/LiCGC | Li] (a) and [Li | P(EO/PO)-PEO<sub>3</sub>/LiCGC | Li] (b) symmetrical cells at 288.15 K. Both of the  $R_b$  values in the high-frequency range and  $R_{Li}$  at the electrolyte–Li metal interface in the low-frequency range were observed in the Cole–Cole plot of the system when  $x = 0$ . The time constants of  $R_b$  and  $R_{Li}$  were kHz order and about 5–10 Hz, respectively, and were calculated when this spectrum was fitted using the equivalent circuit described by Equation (2):

$$Q_b/R_b + Q_{Li}/R_{Li} \quad (2)$$

where  $Q_b$  is the capacitance of the electrolyte bulk. The Nyquist plots of the [Li | composite solid electrolytes ( $x = 50$ –150) | Li] symmetrical cells exhibited a new semicircular arc with an increasing  $x$  value in the intermediate-frequency range between the frequency region of  $R_b$  and  $R_{Li}$ . This semicircular arc indicated the formation of an LICGC continuous phase

into composite solid electrolytes. Therefore, the Nyquist plots for these composite ranges were analyzed using an equivalent circuit described by Equation (3), and  $R_b$ ,  $R_{GB}$ , and  $R_{Li}$  were calculated, respectively.



**Figure 4.** Time dependence of the electrolyte–Li metal interfacial resistance ( $R_{Li}$ ) in the P(EO/PO)/LICGC composite electrolytes at 333.2 K (EO = ethylene oxide; PO = propylene oxide; LICGC =  $Li_{1+x+y}Al_xTi_{2-x}Si_yP_{3-y}O_{12}$ ).

$$Q_b/R_b + Q_{GB}/R_{GB} + Q_{Li}/R_{Li} \quad (3)$$

where  $Q_{GB}$  is the capacitance of the formed grain boundary component. The obtained temperature dependence of  $R_{GB}$  and  $R_{Li}$  was linear and followed the Arrhenius law. The Arrhenius equation expresses the relationship between the rate of a chemical reaction and the apparent activation energy. It is given by Equation (4):

$$k = A \exp(-E_a/RT) \quad (4)$$

where  $k$ ,  $A$ , and  $R$  are the reaction rate constant, the frequency factor, and the gas constant, respectively. The slopes of the lines obtained from the Arrhenius plots of  $R_{GB}$  and  $R_{Li}$  were applied to Equation (4) to calculate  $E_{a,GB}$  and  $E_{a,Li}$ .

Figure 6a shows the dependence of the apparent activation energy ( $E_a$ ) values of  $R_{GB}$  and  $R_{Li}$  on  $x$ . P(EO/PO)/LICGC had the highest  $E_{a,Li}$  value when  $x = 50$ , but the value decreased as  $x$  increased. This suggests that the continuous LICGC phase formed near the electrolyte–Li metal electrode interface as  $x$  increased, and this continuous phase promoted  $Li^+$  transport. The  $E_{a,GB}$  decreased as  $x$  increased ( $x = 50:127 \text{ kJ mol}^{-1}$ ;  $x = 150:96 \text{ kJ mol}^{-1}$ ). This was caused by an increase in the LICGC continuous phase in the electrolyte as  $x$  increased, which facilitated  $Li^+$  transport. The decreases in  $E_{a,Li}$  and  $E_{a,GB}$  indicate that LICGC is a promising material that could enhance the output characteristics of all-solid-state batteries. However, the  $E_{a,Li}$  of P(EO/PO)-PEO<sub>3</sub>/LICGC increased up to  $x = 50$  as the LICGC content of the composite increased, and decreased slightly thereafter. Figure 4 reveals that the  $R_{Li}$  decreased in the composite, and the introduction of PEO<sub>3</sub> may have promoted the frequency factor associated with the electrolyte–Li metal electrode interfacial reaction.

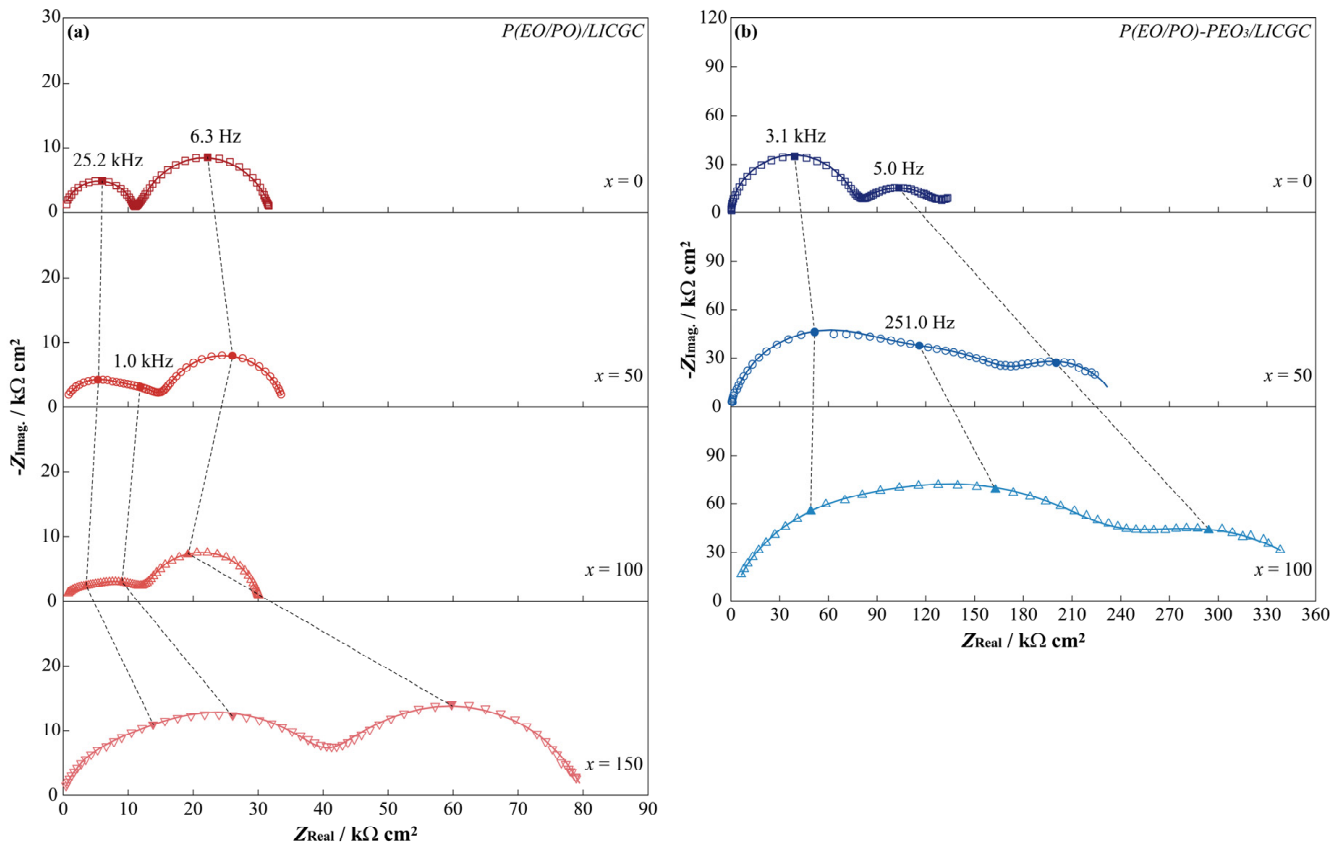


**Figure 5.** Cole–Cole plots of [Li|P(EO/PO)/LiCGC|Li] (a) and [Li|P(EO/PO)/LiCGC|Li] (b) symmetrical cells (a) at 288.15 K (EO = ethylene oxide; PO = propylene oxide; LICGC =  $\text{Li}_{1+x+y}\text{Al}_x\text{Ti}_{2-x}\text{Si}_y\text{P}_{3-y}\text{O}_{12}$ ).

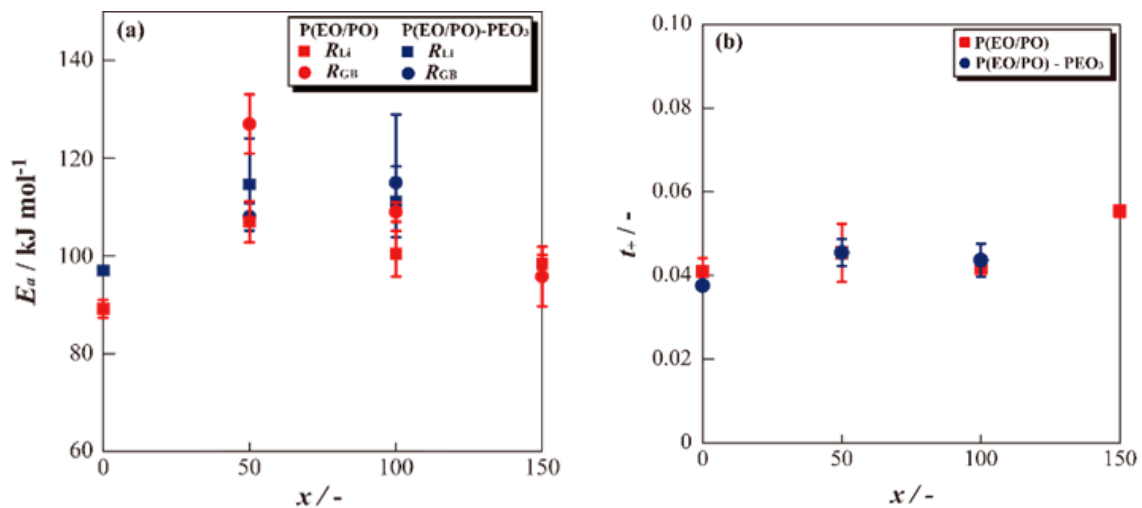


**Figure 6.** Relationships of the apparent activation energies of grain boundary resistance and electrolyte–Li metal interfacial resistance on  $x$  (a) and the  $\text{Li}^+$  transport number ( $t_+$ ) (b) in the P(EO/PO)/LICGC composite electrolytes (EO = ethylene oxide; PO = propylene oxide; LICGC =  $\text{Li}_{1+x+y}\text{Al}_x\text{Ti}_{2-x}\text{Si}_y\text{P}_{3-y}\text{O}_{12}$ ).

The  $\text{Li}^+$  transport number ( $t_+$ ) was measured using a [Li| composite solid electrolyte | Li] symmetrical cell, and the semicircular arcs obtained at the high-frequency side were symmetrical shapes. In contrast, asymmetric arcs were obtained as  $x$  increased. The semicircular arcs obtained on the low-frequency side were attributed to resistance ( $Z_{\text{diff}}$ ) caused by  $\text{Li}^+$

diffusion, and the high- and low-frequency sides were analyzed using the following equivalent circuit described by Equations (5)–(7) to separate the resistance components:

High-frequency side:

$$Q_b/R_b + Q_{Li}/R_{Li} \quad (x = 0) \quad (5)$$

$$Q_b/R_b + Q_{GB}/R_{GB} + Q_{Li}/R_{Li} \quad (x \geq 50) \quad (6)$$

Low-frequency side:

$$R + Q/R + Q_{diff}/Z_{diff} \quad (7)$$

The obtained resistance component was applied to Equation (8) to calculate  $t_+$ .

$$t_+ = R_b / (R_b + Z_{diff}) \quad (8)$$

Figure 6b shows the relationship between  $t_+$  and  $x$  in P(EO/PO)/LICGC and P(EO/PO)-PEO3/LICGC. For both composite solid electrolytes, the  $t_+$  values when  $x = 0$  to 100 were stable, whereas when  $x = 150$ , the  $t_+$  value increased. The introduction of LICGC with a higher  $t_+$  than the polymer phase promoted sufficient  $Li^+$  transport into the composite solid electrolytes by expanding the LICGC continuous phase, even though they had relatively low  $t_+$  values of less than 0.1 [30]. This suggests that the introduction of LICGC into polyether-based solid polymer electrolytes forms a stable interface with the Li metal electrode and promotes  $Li^+$  transport by forming a continuous phase.

### 3.5. Li Precipitation/Dissolution Characteristics in P(NB/G2)/LICGC

Figure 7 shows the cyclic voltammograms of [Li|Ni] cells obtained using P(NB/G2)/LICGC composite electrolytes. In all compositions of P(NB/G2)/LICGC, the reduction currents observed during the reduction processes were attributed to a deposition reaction of the Li (less than 0 V versus  $Li/Li^+$ ). Furthermore, clear oxidation peaks attributable to the dissolution reaction of the deposited Li were confirmed, and the Coulombic efficiencies at  $x = 0, 50$ , and 100 were calculated to be 18.6%, 39.1%, and 21.9%, respectively, from the area ratios of the current peaks related to the Li deposition/dissolution reactions. Because the Coulombic efficiency increased as  $x$  increased, the introduction of LICGC to P(NB/G2) may have suppressed irreversible reactions. This suggests that P(NB/G2)/LICGC acts as a  $Li^+$ -conducting solid electrolyte and has potential for use in all-solid-state batteries.

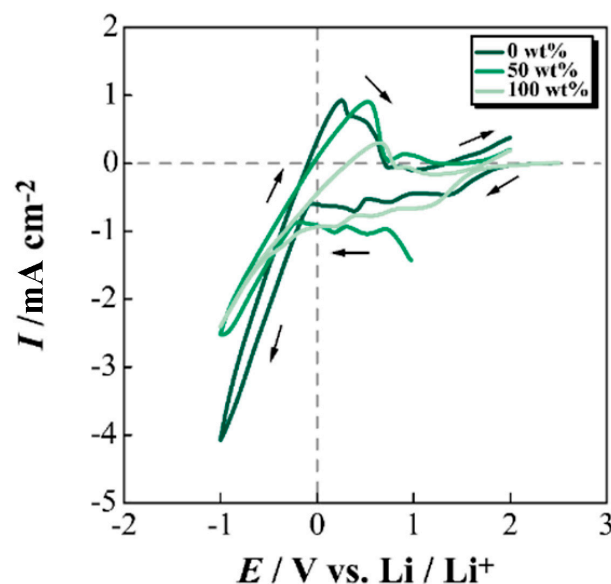


**Figure 7.** Cyclic voltammograms of the P(NB/G2)/LICGC composite solid electrolytes (NB/G2 = norbornene/di-methylene-glycol di-methyl ether; LICGC =  $Li_{1+x+y}Al_xTi_{2-x}Si_yP_{3-y}O_{12}$ ).

#### 4. Conclusions

In the present study, we prepared highly flexible and self-standing chemically cross-linked P(EO/PO)/LICGC electrolytes, branched P(EO/PO)-PEO<sub>3</sub>/LiCGC electrolytes, and physically cross-linked P(NB/G2)/LICGC electrolytes, and evaluated their thermophysical and electrochemical properties via DSC, AC impedance, and cyclic voltammetry. The addition of LICGC to the polymer electrolyte phase contributed sufficiently to the formation of continuous LICGC pathways to prevent grain boundary resistance. Moreover, the stable interfacial formation of Li metal was achieved regardless of the presence of reductive components in the LICGC, and the relatively favorable deposition/dissolution of Li metal on Ni was also confirmed. Therefore, these chemically and physically cross-linked hybrid solid electrolytes are potential candidate materials for the next generation of all-solid-state battery systems.

**Supplementary Materials:** The following supporting information can be downloaded at: <https://www.mdpi.com/article/10.3390/batteries9100492/s1>, Table S1: The  $\sigma$  values of P(EO/PO)/ $x$  wt% LICGC electrolytes at each temperature; Table S2: The  $\sigma$  values of P(EO/PO)-PEO<sub>3</sub>/ $x$  wt% LICGC electrolytes at each temperature; Table S3: The  $\sigma$  values of P(NB/G2)/ $x$  wt% LICGC electrolytes at each temperature.

**Author Contributions:** Conceptualization, S.S.; methodology, S.S.; validation, Y.K. and K.H.; formal analysis, Y.K.; investigation, Y.K.; polymer synthesis, M.M.; writing—original draft preparation, Y.K. and K.H.; writing—review and editing, S.S.; supervision, S.S.; project administration, M.M. and S.S.; funding acquisition, S.S. All authors have read and agreed to the published version of the manuscript.

**Funding:** This work was supported by the Murata Science Foundation and the Iketani Science and Technology Foundation, Japan.

**Data Availability Statement:** The data that support the findings of this study are available from the corresponding author, S.S., upon reasonable request.

**Conflicts of Interest:** The authors declare no conflict of interest.

#### References

1. Tarascon, J.-M.; Armand, M. Issues and Challenges Facing Rechargeable Lithium Batteries. *Nature* **2001**, *414*, 359–367. [CrossRef]
2. Yang, Z.; Zhang, J.; Kintner-Meyer, M.C.W.; Lu, X.; Choi, D.; Lemmon, J.P.; Liu, J. Electrochemical Energy Storage for Green Grid. *Chem. Rev.* **2011**, *111*, 3577–3613. [CrossRef]
3. Wang, J.; Yamada, Y.; Sodeyama, K.; Watanabe, E.; Takada, K.; Tateyama, Y.; Yamada, A. Fire-Extinguishing Organic Electrolytes for Safe Batteries. *Nat. Energy* **2017**, *3*, 22–29. [CrossRef]
4. Manthiram, A.; Yu, X.; Wang, S. Lithium Battery Chemistries Enabled by Solid-State Electrolytes. *Nat. Rev. Mater.* **2017**, *2*, 16103. [CrossRef]
5. Long, L.; Wang, S.; Xiao, M.; Meng, Y. Polymer Electrolytes for Lithium Polymer Batteries. *J. Mater. Chem. A* **2016**, *4*, 10038–10039. [CrossRef]
6. Randau, S.; Weber, D.A.; Kötz, O.; Koerver, R.; Braun, P.; Weber, A.; Ivers-Tiffée, E.; Adermann, T.; Kulisch, J.; Zeier, W.G.; et al. Benchmarking the Performance of All-Solid-State Lithium Batteries. *Nat. Energy* **2020**, *5*, 259–270. [CrossRef]
7. Cavers, H.; Molaiyan, P.; Abdollahifar, M.; Lassi, U.; Kwade, A. Perspectives on Improving the Safety and Sustainability of High Voltage Lithium-Ion Batteries Through the Electrolyte and Separator Region. *Adv. Energy Mater.* **2022**, *12*, 2200147. [CrossRef]
8. Molaiyan, P.; Mailhot, S.E.; Voges, K.; Kantola, A.M.; Hu, T.; Michalowski, P.; Kwade, A.; Telkki, V.-V.; Lassi, U. Investigation of the Structure and Ionic Conductivity of a Li<sub>3</sub>InCl<sub>6</sub> Modified by Dry Room Annealing for Solid-State Li-ion Battery Applications. *Mater. Des.* **2023**, *227*, 111690. [CrossRef]
9. Kamaya, N.; Homma, K.; Yamakawa, Y.; Hirayama, M.; Kanno, R.; Yonemura, M.; Kamiyama, T.; Kato, Y.; Hama, S.; Kawamoto, K.; et al. A Lithium Superionic Conductor. *Nat. Mater.* **2011**, *10*, 682–686. [CrossRef]
10. Muramatsu, H.; Hayashi, A.; Ohtomo, T.; Hama, S.; Tatsumisago, M. Structural Change of Li<sub>2</sub>S–P<sub>2</sub>S<sub>5</sub> Sulfide Solid Electrolytes in the Atmosphere. *Solid State Ion.* **2011**, *182*, 116–119. [CrossRef]
11. Itoh, M.; Inaguma, Y.; Jung, W.H.; Chen, L.; Nakamura, T. High Lithium Ion Conductivity in the Perovskite-Type Compounds Ln<sub>12</sub>Li<sub>12</sub>TiO<sub>3</sub> (Ln=La,Pr,Nd,Sm). *Solid State Ion.* **1994**, *70–71*, 203–207. [CrossRef]
12. Murugan, R.; Thangadurai, V.; Weppner, W. Fast Lithium Ion Conduction in Garnet-Type Li<sub>7</sub>La<sub>3</sub>Zr<sub>2</sub>O<sub>12</sub>. *Angew. Chem. Int. Ed.* **2007**, *46*, 7778–7781. [CrossRef] [PubMed]
13. Breuer, S.; Prutsch, D.; Ma, Q.; Epp, V.; Preishuber-Pflügl, F.; Tietz, F.; Wilkening, M. Separating Bulk from Grain Boundary Li Ion Conductivity in the Sol-Gel Prepared Solid Electrolyte Li<sub>1.5</sub>Al<sub>0.5</sub>Ti<sub>1.5</sub>(PO<sub>4</sub>)<sub>3</sub>. *J. Mater. Chem. A* **2015**, *3*, 21343–21350. [CrossRef]

14. Ioanniti, M.M.; Tenhaeff, W.E. Enhancing the Stability of Lithium Ion  $\text{Li}_{1+x+y}\text{Al}_x\text{Ti}_{2-x}\text{Si}_y\text{P}_{3-y}\text{O}_{12}$  Glass–Ceramic Conductors in Aqueous Electrolytes. *J. Power Sources* **2017**, *371*, 209–216. [[CrossRef](#)]
15. Xu, X.; Wen, Z.; Wu, X.; Yang, X.; Gu, Z. Lithium Ion-Conducting Glass-Ceramics of  $\text{Li}_{1.5}\text{Al}_{0.5}\text{Ge}_{1.5}(\text{PO}_4)_3\text{-XLi}_2\text{O}$  ( $X=0.0\text{-}0.20$ ) with Good Electrical and Electrochemical Properties. *J. Am. Ceram. Soc.* **2007**, *90*, 2802–2806. [[CrossRef](#)]
16. Takada, K.; Kondo, S. Lithium Ion Conductive Glass and Its Application to Solid State Batteries. *Ionics* **1998**, *4*, 42–47. [[CrossRef](#)]
17. Fu, J. Superionic Conductivity of Glass-Ceramics in the System  $\text{Li}_2\text{O-Al}_2\text{O}_3\text{-TiO}_2\text{-P}_2\text{O}_5$ . *Solid State Ion.* **1997**, *96*, 195–200. [[CrossRef](#)]
18. Seino, Y.; Ota, T.; Takada, K.; Hayashi, A.; Tatsumisago, M. A Sulphide Lithium Super Ion Conductor Is Superior to Liquid Ion Conductors for Use in Rechargeable Batteries. *Energy Environ. Sci.* **2014**, *7*, 627–631. [[CrossRef](#)]
19. Armand, M. The History of Polymer Electrolytes. *Solid State Ion.* **1994**, *69*, 309–319. [[CrossRef](#)]
20. Fan, L.; Wei, S.; Li, S.; Li, Q.; Lu, Y. Recent Progress of the Solid-State Electrolytes for High-Energy Metal-Based Batteries. *Adv. Energy Mater.* **2018**, *8*, 1702657. [[CrossRef](#)]
21. Bouchet, R.; Lascaud, S.; Rosso, M. An EIS Study of the Anode Li/PEO-LiTFSI of a Li Polymer Battery. *J. Electrochem. Soc.* **2003**, *150*, A1385. [[CrossRef](#)]
22. Xue, Z.; He, D.; Xie, X. Poly(Ethylene Oxide)-Based Electrolytes for Lithium-Ion Batteries. *J. Mater. Chem. A* **2015**, *3*, 19218–19253. [[CrossRef](#)]
23. Nishimoto, A.; Agehara, K.; Furuya, N.; Watanabe, T.; Watanabe, M. High Ionic Conductivity of Polyether-Based Network Polymer Electrolytes with Hyperbranched Side Chains. *Macromolecules* **1999**, *32*, 1541–1548. [[CrossRef](#)]
24. Zou, Z.; Li, Y.; Lu, Z.; Wang, D.; Cui, Y.; Guo, B.; Li, Y.; Liang, X.; Feng, J.; Li, H.; et al. Mobile Ions in Composite Solids. *Chem. Rev.* **2020**, *120*, 4169–4221. [[CrossRef](#)] [[PubMed](#)]
25. Zhao, Y.; Wu, C.; Peng, G.; Chen, X.; Yao, X.; Bai, Y.; Wu, F.; Chen, S.; Xu, X. A New Solid Polymer Electrolyte Incorporating  $\text{Li}_{10}\text{GeP}_2\text{S}_{12}$  into a Polyethylene Oxide Matrix for All-Solid-State Lithium Batteries. *J. Power Sources* **2016**, *301*, 47–53. [[CrossRef](#)]
26. Fu, K.; Gong, Y.; Dai, J.; Gong, A.; Han, X.; Yao, Y.; Wang, C.; Wang, Y.; Chen, Y.; Yan, C.; et al. Flexible, Solid-State, Ion-Conducting Membrane with 3D Garnet Nanofiber Networks for Lithium Batteries. *Proc. Natl. Acad. Sci. USA* **2016**, *113*, 7094–7099. [[CrossRef](#)]
27. Zhu, P.; Yan, C.; Dirican, M.; Zhu, J.; Zang, J.; Selvan, R.K.; Chung, C.C.; Jia, H.; Li, Y.; Kiyak, Y.; et al.  $\text{Li}_{0.33}\text{La}_{0.557}\text{TiO}_3$  Ceramic Nanofiber-Enhanced Polyethylene Oxide-Based Composite Polymer Electrolytes for All-Solid-State Lithium Batteries. *J. Mater. Chem. A* **2018**, *6*, 4279–4285. [[CrossRef](#)]
28. Chen, F.; Yang, D.; Zha, W.; Zhu, B.; Zhang, Y.; Li, J.; Gu, Y.; Shen, Q.; Zhang, L.; Sadoway, D.R. Solid Polymer Electrolytes Incorporating Cubic  $\text{Li}_7\text{La}_3\text{Zr}_2\text{O}_{12}$  for All-Solid-State Lithium Rechargeable Batteries. *Electrochim. Acta* **2017**, *258*, 1106–1114. [[CrossRef](#)]
29. Karthik, K.; Murugan, R. Lithium Garnet Based Free-Standing Solid Polymer Composite Membrane for Rechargeable Lithium Battery. *J. Solid State Electrochem.* **2018**, *22*, 2989–2998. [[CrossRef](#)]
30. Kato, M.; Hiraoka, K.; Seki, S. Investigation of the Ionic Conduction Mechanism of Polyether/ $\text{Li}_7\text{La}_3\text{Zr}_2\text{O}_{12}$  Composite Solid Electrolytes by Electrochemical Impedance Spectroscopy. *J. Electrochem. Soc.* **2020**, *167*, 070559. [[CrossRef](#)]
31. Chen, L.; Li, Y.; Li, S.P.; Fan, L.Z.; Nan, C.W.; Goodenough, J.B. PEO/Garnet Composite Electrolytes for Solid-State Lithium Batteries: From “Ceramic-in-Polymer” to “Polymer-in-Ceramic”. *Nano Energy* **2018**, *46*, 176–184. [[CrossRef](#)]
32. Otake, Y.; Hiraoka, K.; Takahashi, K.; Ohashi, S.; Matsuyama, M.; Kubota, S.; Kato, Y.; Seki, S. Effects of Molecular Structure of Cross-Linked Solid Polymer Electrolytes on Ionic Conduction Behavior. *J. Electrochem. Soc.* **2023**, *170*, 040510. [[CrossRef](#)]
33. Piana, G.; Bella, F.; Geobaldo, F.; Meligrana, G.; Gerbaldi, C. PEO/LAGP Hybrid Solid Polymer Electrolytes for Ambient Temperature Lithium Batteries by Solvent-Free, “One Pot” Preparation. *J. Energy Storage* **2019**, *26*, 100947. [[CrossRef](#)]
34. Lee, J.; Howell, T.; Rottmayer, M.; Boeckl, J.; Huang, H. Free-Standing PEO/LiTFSI/LAGP Composite Electrolyte Membranes for Applications to Flexible Solid-State Lithium-Based Batteries. *J. Electrochem. Soc.* **2019**, *166*, A416–A422. [[CrossRef](#)]
35. Hartmann, P.; Leichtweiss, T.; Busche, M.R.; Schneider, M.; Reich, M.; Sann, J.; Adelhelm, P.; Janek, J. Degradation of NASICON-Type Materials in Contact with Lithium Metal: Formation of Mixed Conducting Interphases (MCI) on Solid Electrolytes. *J. Phys. Chem. C* **2013**, *117*, 21064–21074. [[CrossRef](#)]

**Disclaimer/Publisher’s Note:** The statements, opinions and data contained in all publications are solely those of the individual author(s) and contributor(s) and not of MDPI and/or the editor(s). MDPI and/or the editor(s) disclaim responsibility for any injury to people or property resulting from any ideas, methods, instructions or products referred to in the content.